Turkish Journal of Civil Engineering, 2025, 51-74, Paper 793, ***Research Article***

Mixed Finite Elements for Higher-order Laminated Cylindrical and Spherical Shells

Yonca BAB[1*]
Akif KUTLU[2]

ABSTRACT

This paper presents a mixed finite element (MFE) formulation for studying the linear static behavior of both thin and relatively thick laminated composite cylindrical and spherical shells. The method employs the Higher Order Shear Deformation Theory to account for cross-section warping due to transverse shear stress. It ensures the stationarity of the system's functional using the Hellinger-Reissner principle. Finite element discretization is accomplished with four-noded quadrilateral two-dimensional elements. The MFE formulation offers the advantage of directly obtaining displacements and stress resultants at the nodes. Comparison and convergence analyses are performed considering various shear functions, boundary conditions, and geometrical configurations.

Keywords: Higher order shear deformation theory, laminated composite shell, Hellinger-Reissner principle, mixed finite element method, static analysis.

1. INTRODUCTION

Laminated composite shells, as fundamental thin-walled structural elements, find frequent applications in various industries owing to their inherent advantages. These shells are typically composed of different material layers and play a pivotal role in sectors such as construction, aviation, automotive, and marine industries. The history of laminated composite shells dates back to the mid-20th century when researchers began combining diverse materials to attain superior performance characteristics. This includes achieving a high strength-to-weight ratio, robust resistance to corrosion, fatigue, and impact, enhanced design flexibility, improved energy efficiency etc. Load-bearing capacity, damage initiation, and failure load are crucial considerations in the design of composite materials. Thus, ensuring structural integrity necessitates a comprehensive mechanical analysis. Although

Note:
- This paper was received on November 17, 2023 and accepted for publication by the Editorial Board on July 19, 2024.
- Discussions on this paper will be accepted by March 31, 2025.
- https://doi.org/10.18400/tjce.1396909

1 Istanbul Technical University, Department of Civil Engineering, Istanbul, Türkiye
bab@itu.edu.tr - https://orcid.org/0000-0002-1807-9306

2 Istanbul Technical University, Department of Civil Engineering, Istanbul, Türkiye
kutluak@itu.edu.tr - https://orcid.org/0000-0001-6865-3022

* Corresponding author

experimental analyses may be considered as an option for mechanical investigations, due to practical constraints, whether financial or physical, the feasibility of conducting experimental analyses is often limited. Theoretical approaches stand out for the assessment of structural systems as they provide a comprehensive environment regarding various scenarios. Numerous studies in the literature explore the effectiveness of the theories developed for the mechanical analyses of laminated structures and try to improve their accuracy further. Several prominent theories in structural analysis include Classical Lamination Theory (CLT), First-Order Shear Deformation Theory (FSDT), Higher-Order Shear Deformation Theory (HSDT), and Zigzag Theories (ZZ) [1,2].

Reddy and Chandrashekhara [3] employed FSDT to create a finite element for analyzing geometrically non-linear transient responses of laminated composite spherical and cylindrical shells. Hossain et al. [4] examined numerical analysis of laminated spherical shells applying FSDT. Asadi and Qatu [5] examined static response of thick laminated composite cylindrical shells using two First Order Shear Deformation Theories (FSDTs), with results compared to existing literature and 3D analysis for validation. Khdeir [6] obtained exact solutions for the free vibration and static deflection of cross-ply laminated cylindrical panels and circular cylindrical shells using deep FSDT. Mousavi and Aghdam [7] applied the differential cubature method and FSDT to analyze the bending of laminated cylindrical panels with various boundary conditions and loads.

Sobhaniaragh et al. [8] employed the thermal response of nanocomposite cylindrical shells reinforced by aggregated Carbon Nanotubes adopting Reddy's Third-Order Shear Deformation Theory (TSDT). Reddy and Liu [9] presented a pioneering study that carried out the static and dynamic analysis of laminated composite spherical and cylindrical shells using HSDT. Sayyad and Ghugal [10] and Mantari et al. [11] obtained analytical solutions for static analyses of laminated spherical shells based on HSDT. Kumar et al. [12] investigated static behavior of laminated composite spherical, cylindrical, conical and hyper shells based on FEM and HSDT. Giunta et al. [13] implemented Carrera's Unified Formulation (CUF) for laminated spherical shells. Asadi et al. [14], Ton-that et al. [15] and Zuo et al. [16] used different theories in the static and dynamic analysis of laminated composite shells. Yaghoubshahi et al. [17] applied HSDT to analyze laminated shells, resulting in a system of 31 differential equations solved numerically for various shell configurations, with results validated against ANSYS software. Groh and Weaver [18] addressed static inconsistencies in certain HSDTs applied to beams, plates, and cylindrical shells with clamped boundaries, highlighting inaccuracies in vanishing Kirchhoff rotation conditions and proposing improved formulations to correct these shortfalls. Bhaskar and Varadan [19] implemented HSDT for analyzing laminated anisotropic cylindrical shells of revolution, based on realistic in-plane displacement approximations, validated against 3D elasticity results, and applied to an isoparametric FEM. Doan et al. [20] explored stress concentration in cylinder laminated shells due to force and structural variations based on Quasi-3D HSDT. Viola et al. [21] presented static behavior of doubly-curved laminated composite shells and panels using a 2D HSDT and Generalized Differential Quadrature (GDQ) technique. Pinto Correia et al. [22] presented an isoparametric FE for static, dynamic and buckling analyses of laminated conical shell panels based on HSDT. It supports static analysis, eigenvalue problems, and demonstrates with illustrative examples. Tornabene et al. [23] investigated the recovery of through-the-thickness transverse strains and stresses in functionally graded doubly-curved sandwich shell structures applying HSDT and CUF.

Yasin and Kapuria [24] employed the ZZ to analyze the static and dynamic behavior of singly- and doubly-curved composite and sandwich shallow shells. Gupta and Pradyumna [25] worked also on ZZ for the bending analysis of variable stiffness laminated spherical, cylindrical and hyperboloid shells. Examples of various studies dealing with different aspects of shell analysis are given next.

Kulikov and Plotnikova [26] extended Sampling Surfaces (SaS) method to cylindrical and spherical laminated composite shells to solve 3D elasticity problems accurately by using strategically placed SaS. Qatu and Algothani [27] employed a consistent set of equations to derive exact solutions for isotropic and laminated composite plates and cylindrical shallow shells. They applied the Ritz method and finite elements to compare the static behavior. Karatas and Yukseler [28] presented the snap-through buckling behavior of rigid vinyl polyethylene shallow spherical shells subjected to static ring loads using finite difference and the Newton-Raphson Method. Sofiyev et al. [29] investigated the torsional stability of non-homogeneous orthotropic composite cylindrical shells within an elastic medium.

Some recent studies on the laminated shell analysis include Yadav et al. [30], where the authors analyzed the dynamic instability and nonlinear vibrations of fluid-filled laminated composite cylindrical shells under harmonic axial loading, considering skew modes and using HSDT. Ray [31] provided three-dimensional exact solutions for the static analysis of spherical, paraboloid and hyperboloid antisymmetric angle-ply composite shells. Alam et al. [32] introduced a modified higher-order zigzag theory for the static analysis of laminated cylindrical and spherical composite/sandwich shells. Arumugam et al. [33] formulated the vibration and damping characteristics of reinforced laminated composite cylindrical sandwich shells adopting HSDT and FE. Within the realm of FE formulations, mixed methodologies have been utilized in numerous investigations on structures in existing literature, and a few of these is provided below.

Ozutok and Madenci [34] combined the mixed finite element method (MFEM) with HSDT for static analysis of laminated composite beams. Kutlu et al. [35–37] and Aribas et al. [38–40] have illustrated the benefits of MFEM-derived formulations while precisely predicting stress resultants and components in diverse structural configurations. Kutlu and Omurtag [41] applied a MFE formulation based on the Hellinger-Reissner principle for the static behavior of elliptic plates under large deflection conditions. Omurtag and Akoz [42] introduced a computational procedure and a mixed finite element (ORTH036) for orthotropic cylindrical shells.

In this study, the mixed finite element formulation for laminated composite beams based on HSDT is extended, as originally derived by Bab and Kutlu [43,44], to perform static analyses on laminated spherical and cylindrical shells. For the higher order terms, shear functions suggested by Touratier [45], Reddy [46], Reissner [47] and Nguyen Xuan et al. [48] are conducted. The Hellinger-Reissner principle is employed to describe the energy expression of the spherical shell and reduced for the cylindrical shell. In the displacement field, three displacement and two rotation terms are taken into account. The generated mixed finite element functional contains quantities in terms of displacements and stress resultants. During the generation of finite element system equations, quadrilateral four-node elements are described with bi-linear shape functions. By solving the finite element equations, displacement and rotation components, as well as force and moment type quantities, are obtained directly at the nodes. In this way, strain measurements are calculated using

compliance matrices without using derivatives at the nodes. Convergence analyses are performed by increasing the element density in the meshes. Comparison analyses are carried out with static solutions in the literature. Several solutions are presented in various lamination, loading and boundary conditions to show the effectiveness of the proposed numerical procedure on the analyses of laminated composite shell structures.

2. FIELD EQUATIONS AND NUMERICAL FORMULATION

Considering the higher order shear effect, the displacement field of the laminated composite spherical shell (Figure 1a) can be described as follows:

$$\begin{aligned} u^*(x,y,z) &= (1+\frac{z}{R_x})u(x,y) - z\,w_{,x}(x,y) + f(z)\theta_x(x,y) \\ v^*(x,y,z) &= (1+\frac{z}{R_y})v(x,y) - z\,w_{,y}(x,y) + f(z)\theta_y(x,y) \\ w^*(x,y,z) &= w(x,y) \end{aligned} \tag{1}$$

Here, $u^*(x,y,z)$ and $v^*(x,y,z)$ denote axial displacement field and $w^*(x,y,z)$ denotes the transverse displacement field of the shell. $u(x,y)$ and $v(x,y)$ are the axial displacements and $w(x,y)$ is the deflection of the shell at its mid-surface where x and y are curvilinear orthogonal coordinates defined at the mid-surface of the shell. z is the coordinate in the direction of shell thickness (Figure 1b). Also, $\theta_x(x,y)$ describes the rotation of the section about the y -axis and $\theta_y(x,y)$ describes the rotation of the section about the x -axis. R_x and R_y are the radii of curvatures of the spherical shell. When the formulation is reduced to the cylindrical shell, $R_x = \infty$ is imposed, therefore in Equation (1) only y represent the curvilinear coordinate, x reduces to a straight coordinate axis. In addition, $f(z)$ is called the shear function that configures stress and strain distribution along the thickness of

Table 1 - Shear functions used in this study

Researcher	$f(z)$	Shell type
Touratier [45]	$\frac{h}{\pi}\sin\left(\frac{\pi}{h}z\right)$	Cylindrical+Spherical
Reddy [46]	$z\left(1-\frac{4z^2}{3h^2}\right)$	Cylindrical+Spherical
Reissner [47]	$\frac{5z}{4}\left(1-\frac{4z^2}{3h^2}\right)$	Cylindrical
Nguyen-Xuan et al. [48]	$\frac{7}{8}z-\frac{2}{h^2}z^3+\frac{2}{h^4}z^5$	Cylindrical

the structure. Type of those functions can be noticed as polynomial, exponential or trigonometrical. In the current study, some of those functions used in analyses can be found in Table 1 where h refers to the section thickness:

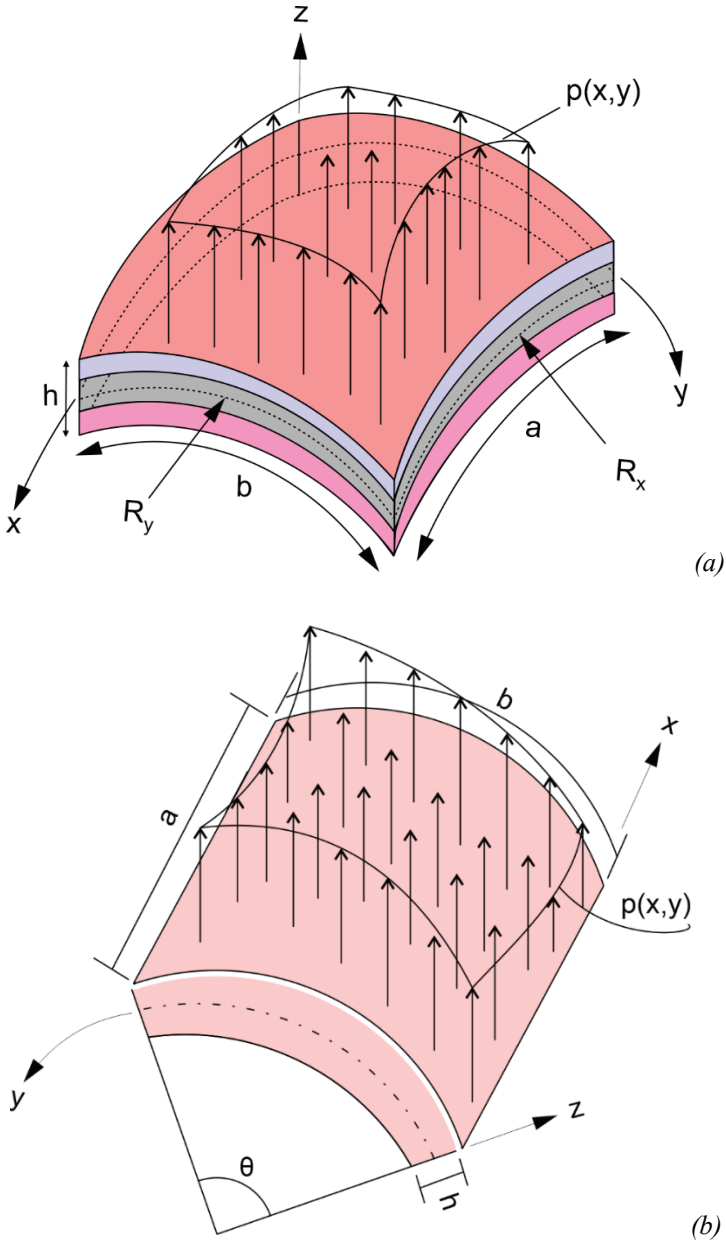

Figure 1 - a) Spherical shell coordinate system b) Cylindrical shell coordinate system

In an orthogonal curvilinear coordinate system, the engineering shear strain and linear normal components are expressed as follows [49]:

$$\begin{aligned}\varepsilon_i &= \frac{\partial}{\partial \xi_i}\left(\frac{u_i}{A_i}\right)+\frac{1}{A_i}\sum_{k=1}^{3}\frac{u_k}{A_k}\frac{\partial A_i}{\partial \xi_k}\\ \gamma_{ij} &= \frac{1}{A_i A_j}\left[A_1^{\,2}\frac{\partial}{\partial \xi_j}\left(\frac{u_i}{A_i}\right)+A_j^{\,2}\frac{\partial}{\partial \xi_i}\left(\frac{u_j}{A_j}\right)\right]\quad (i\neq j)\end{aligned} \tag{2}$$

Where

$$\xi_3=\zeta\ ,\quad A_1=a_1\left(1+\frac{\zeta}{R_1}\right)\quad ,\quad A_2=a_2\left(1+\frac{\zeta}{R_2}\right) \tag{3}$$

and a_α $(\alpha=1,2)$ represent the square root of the surface metric tensor ($g_{\alpha\beta}$, $(\alpha,\beta=1,2)$), see Equation (4).

$$g_{\alpha\beta}=g_\alpha.g_\beta\quad ,\quad a_\alpha=\sqrt{g_{\alpha\alpha}} \tag{4}$$

In Equation (4), g_1 and g_2 represent the tangent lines of the ξ_1 and ξ_2 axes, respectively.

The conversion of Reddy's [49] notation in the Equation (2) to the notation here is:

$$\begin{aligned}&\xi_1=x\ ,\ \xi_2=y\ ,\ \zeta=z\ ,\ \varepsilon_1=\varepsilon_{xx}\ ,\ \varepsilon_2=\varepsilon_{yy}\ ,\ \varepsilon_3=\varepsilon_{zz}\ ,\ u_1=u\ ,\ u_2=v\ ,\ u_3=w\\ &\gamma_{12}=\gamma_{xy}\ ,\ \gamma_{13}=\gamma_{xz}\ ,\ \gamma_{23}=\gamma_{yz}\end{aligned} \tag{5}$$

As a sum of above equations, the linear strain components are expressed by Equation (6).

$$\begin{aligned}\varepsilon_{xx} &= u_{,x}-z\,w_{,xx}+\frac{w}{R_x}+f(z)\theta_{x,x}\\ \varepsilon_{yy} &= v_{,y}-z\,w_{,yy}+\frac{w}{R_y}+f(z)\theta_{y,y}\\ \gamma_{xy} &= u^*_{,y}+v^*_{,x}=u_{,y}+v_{,x}-2z\,w_{,xy}+f(z)\left(\theta_{x,y}+\theta_{y,x}\right)\\ \gamma_{yz} &= v^*_{,z}+w^*_{,y}=f_{,z}(z)\theta_y\left(x,y\right)\\ \gamma_{xz} &= u^*_{,z}+w^*_{,x}=f_{,z}(z)\theta_x\left(x,y\right)\end{aligned} \tag{6}$$

The relationship between strain measures and stress resultants is expressed over sectional compliance terms in explicit form as shown in Equation (7).

$$\begin{Bmatrix} u_{,x}+w/R_x \\ v_{,y}+w/R_y \\ u_{,y}+v_{,x} \\ -w_{,xx} \\ -w_{,yy} \\ -2w_{,xy} \\ \theta_{x,x} \\ \theta_{y,y} \\ \theta_{x,y}+\theta_{y,x} \\ \theta_y \\ \theta_x \end{Bmatrix} = \begin{bmatrix} A'_{11} & A'_{12} & A'_{16} & B'_{11} & B'_{12} & B'_{16} & E'_{11} & E'_{12} & E'_{16} & 0 & 0 \\ A'_{12} & A'_{22} & A'_{26} & B'_{12} & B'_{22} & B'_{26} & E'_{12} & E'_{22} & E'_{26} & 0 & 0 \\ A'_{16} & A'_{26} & A'_{66} & B'_{16} & B'_{26} & B'_{66} & E'_{16} & E'_{26} & E'_{66} & 0 & 0 \\ B'_{11} & B'_{12} & B'_{16} & D'_{11} & D'_{12} & D'_{16} & F'_{11} & F'_{12} & F'_{16} & 0 & 0 \\ B'_{12} & B'_{22} & B'_{26} & D'_{12} & D'_{22} & D'_{26} & F'_{12} & F'_{22} & F'_{26} & 0 & 0 \\ B'_{16} & B'_{26} & B'_{66} & D'_{16} & D'_{26} & D'_{66} & F'_{16} & F'_{26} & F'_{66} & 0 & 0 \\ E'_{11} & E'_{12} & E'_{16} & F'_{11} & F'_{12} & F'_{16} & H'_{11} & H'_{12} & H'_{16} & 0 & 0 \\ E'_{12} & E'_{22} & E'_{26} & F'_{12} & F'_{22} & F'_{26} & H'_{12} & H'_{22} & H'_{26} & 0 & 0 \\ E'_{16} & E'_{26} & E'_{66} & F'_{16} & F'_{26} & F'_{66} & H'_{16} & H'_{26} & H'_{66} & 0 & 0 \\ 0 & 0 & 0 & 0 & 0 & 0 & 0 & 0 & 0 & A'^{s}_{44} & A'^{s}_{45} \\ 0 & 0 & 0 & 0 & 0 & 0 & 0 & 0 & 0 & A'^{s}_{45} & A'^{s}_{55} \end{bmatrix} \begin{Bmatrix} N_{xx} \\ N_{yy} \\ N_{xy} \\ M_{xx} \\ M_{yy} \\ M_{xy} \\ M^{f}_{xx} \\ M^{f}_{yy} \\ M^{f}_{xy} \\ Q_{yz} \\ Q_{xz} \end{Bmatrix} \tag{7}$$

Details about the calculation of the sectional compliance terms $(A'_{ij}, B'_{ij}, D'_{ij}, E'_{ij}, F'_{ij}, H'_{ij}, A'^{s}_{ij})$ can be found in the laminated composite plate section of Bab [50]. The linear equilibrium equations for the spherical shell are as described below:

$$\begin{aligned} &q_x + N_{xx,x} + N_{xy,y} = 0 \quad ; \quad q_y + N_{xy,x} + N_{yy,y} = 0 \\ &q_z + M_{xx,xx} + M_{yy,yy} + 2M_{xy,xy} - \frac{N_{xx}}{R_x} - \frac{N_{yy}}{R_y} = 0 \\ &M^{f}_{xx,x} + M^{f}_{xy,y} - Q_{xz} = 0 \quad ; \quad M^{f}_{yy,y} + M^{f}_{xy,x} - Q_{yz} = 0 \end{aligned} \tag{8}$$

The boundary conditions for the spherical shell can be obtained as follows:

$$\begin{aligned} &N_{xx}n_x + N_{xy}n_y = 0 && \text{or} \quad \delta u = 0 \\ &N_{xy}n_x + N_{yy}n_y = 0 && \text{or} \quad \delta v = 0 \\ &M_{xx,x}n_x + M_{yy,y}n_y + 2M_{xy,x}n_y = 0 && \text{or} \quad \delta w = 0 \\ &M^{f}_{xx}n_x + M^{f}_{xy}n_y = 0 && \text{or} \quad \delta\theta_x = 0 \\ &M^{f}_{xy}n_x + M^{f}_{yy}n_y = 0 && \text{or} \quad \delta\theta_y = 0 \end{aligned} \tag{9}$$

According to the Hellinger-Reissner principle, the stationarity condition of the functional of a mechanical problem can be written as in Equation (10).

$$\delta\Pi_{HR} = \int_V \left(\boldsymbol{\varepsilon}^{\mathbf{u}} - \boldsymbol{\varepsilon}^{\boldsymbol{\sigma}}\right)^T \delta\boldsymbol{\sigma}^{\boldsymbol{\sigma}} \mathrm{d}V + \int_V \left(\left(\boldsymbol{\sigma}^{\boldsymbol{\sigma}}\right)^T \delta\boldsymbol{\varepsilon}^{\mathbf{u}} - \mathbf{q}^T\delta\mathbf{u}\right)\mathrm{d}V - \int_\Gamma \hat{\mathbf{t}}^T\delta\mathbf{u}\,\mathrm{d}\Gamma = 0 \tag{10}$$

In Equation (10), the first integral corresponds to the weak form of the compatibility conditions of the strain field $(\boldsymbol{\varepsilon})$, while the second integral expresses the weak form of the equilibrium equations under external load $\mathbf{q}$ under volume integral V. The last integral

shows the work done by the stresses ($\hat{\mathbf{t}}$) at the boundaries (Γ). As a result of using Equations (7) and (8) in Equation (10) and applying integration by parts to eliminate the doubly-differentiated terms, the final form of the functional becomes as follows:

$$
\begin{aligned}
&\int_A \left[u_{,x} \frac{w}{R_x} - \begin{pmatrix} A'_{11}N_{xx} + A'_{12}N_{yy} + A'_{16}N_{xy} + B'_{11}M_{xx} + B'_{12}M_{yy} + B'_{16}M_{xy} \\ + E'_{11}M^f_{xx} + E'_{12}M^f_{yy} + E'_{16}M^f_{xy} \end{pmatrix} \right] \delta N_{xx} \mathrm{d}A \\
&+ \int_A \left[v_{,y} + \frac{w}{R_y} - \begin{pmatrix} A'_{12}N_{xx} + A'_{22}N_{yy} + A'_{26}N_{xy} + B'_{12}M_{xx} + B'_{22}M_{yy} + B'_{26}M_{xy} \\ + E'_{12}M^f_{xx} + E'_{22}M^f_{yy} + E'_{26}M^f_{xy} \end{pmatrix} \right] \delta N_{yy} \mathrm{d}A \\
&+ \int_A \left[u_{,y} + v_{,x} - \begin{pmatrix} A'_{16}N_{xx} + A'_{26}N_{yy} + A'_{66}N_{xy} + B'_{16}M_{xx} + B'_{26}M_{yy} + B'_{66}M_{xy} \\ + E'_{16}M^f_{xx} + E'_{26}M^f_{yy} + E'_{66}M^f_{xy} \end{pmatrix} \right] \delta N_{xy} \mathrm{d}A \\
&+ \int_A \left[w_{,x} \delta M_{xx,x} - \begin{pmatrix} B'_{16}N_{xx} + B'_{26}N_{yy} + B'_{66}N_{xy} + D'_{16}M_{xx} + D'_{26}M_{yy} + D'_{66}M_{xy} \\ + F'_{16}M^f_{xx} + F'_{26}M^f_{yy} + F'_{66}M^f_{xy} \end{pmatrix} \delta M_{xx} \right] \mathrm{d}A \\
&+ \int_A \left[w_{,y} \delta M_{yy,y} - \begin{pmatrix} B'_{12}N_{xx} + B'_{22}N_{yy} + B'_{26}N_{xy} + D'_{12}M_{xx} + D'_{22}M_{yy} + D'_{26}M_{xy} \\ + F'_{12}M^f_{xx} + F'_{22}M^f_{yy} + F'_{26}M^f_{xy} \end{pmatrix} \delta M_{yy} \right] \mathrm{d}A \\
&+ \int_A \left[w_{,x} \delta M_{xy,y} + w_{,y} \delta M_{xy,x} - \begin{pmatrix} B'_{16}N_{xx} + B'_{26}N_{yy} + B'_{66}N_{xy} + D'_{16}M_{xx} + D'_{26}M_{yy} \\ + D'_{66}M_{xy} + F'_{16}M^f_{xx} + F'_{26}M^f_{yy} + F'_{66}M^f_{xy} \end{pmatrix} \delta M_{xy} \right] \mathrm{d}A \\
&+ \int_A \left[\theta_{x,x} - \begin{pmatrix} E'_{11}N_{xx} + E'_{12}N_{yy} + E'_{16}N_{xy} + F'_{11}M_{xx} + F'_{12}M_{yy} + F'_{16}M_{xy} \\ + H'_{11}M^f_{xx} + H'_{12}M^f_{yy} + H'_{16}M^f_{xy} \end{pmatrix} \right] \delta M^f_{xx} \mathrm{d}A \\
&+ \int_A \left[\theta_{y,y} - \begin{pmatrix} E'_{12}N_{xx} + E'_{22}N_{yy} + E'_{26}N_{xy} + F'_{12}M_{xx} + F'_{22}M_{yy} + F'_{26}M_{xy} \\ + H'_{12}M^f_{xx} + H'_{22}M^f_{yy} + H'_{26}M^f_{xy} \end{pmatrix} \right] \delta M^f_{yy} \mathrm{d}A \\
&+ \int_A \left[\theta_{x,y} + \theta_{y,x} - \begin{pmatrix} E'_{16}N_{xx} + E'_{26}N_{yy} + E'_{66}N_{xy} + F'_{16}M_{xx} + F'_{26}M_{yy} + F'_{66}M_{xy} \\ + H'_{16}M^f_{xx} + H_{26}M^f_{yy} + H'_{66}M^f_{xy} \end{pmatrix} \right] \delta M^f_{xy} \mathrm{d}A \\
&+ \int_A \left[\theta_y - \left(A'^s_{44}Q_{yz} + A'^s_{45}Q_{xz} \right) \right] \delta Q_{yz} \mathrm{d}A + \int_A \left[\theta_x - \left(A'^s_{45}Q_{yz} + A'^s_{55}Q_{xz} \right) \right] \delta Q_{xz} \mathrm{d}A - \int_A \delta w q_z \mathrm{d}A \\
&+ \int_A \begin{pmatrix} N_{xx}\delta u_{,x} + M_{xx,x}\delta w_{,x} + M^f_{xx}\delta\theta_{x,x} + N_{yy}\delta v_{,y} + M_{yy,y}\delta w_{,y} + M^f_{yy}\delta\theta_{y,y} + N_{xy}\delta u_{,y} \\ + N_{xy}\delta v_{,x} + M_{xy,x}\delta w_{,y} + M_{xy,y}\delta w_{,x} + M^f_{xy}\delta\theta_{x,y} + M^f_{xy}\delta\theta_{y,x} + Q_{yz}\delta\theta_y + Q_{xz}\delta\theta_x \end{pmatrix} \mathrm{d}A \\
&+ \int_A \left[(N_{xx}/R_x + N_{yy}/R_y)\delta w \right] \mathrm{d}A - \int_\Gamma \hat{t}_i \delta u_i \mathrm{d}\Gamma = 0
\end{aligned}
\tag{11}
$$

Two-dimensional four-node quadrilateral elements (Figure 2) with associated bi-linear shape functions are employed in finite element discretization. The interpolation of field variables occurs through local coordinates, denoted ξ and η, within the master element, where

$-1 \le \xi \le 1$ and $-1 \le \eta \le 1$. The computation involves numerical integrals over a transformation T_e from the master element domain Ω to the element domain Ω_e. The expression for the shape function family is provided by:

$$\varphi_i(\xi,\eta) = \tfrac{1}{4}\left(1+\xi\xi_i\right)\left(1+\eta\eta_i\right), \quad i = (1,...,4) \tag{12}$$

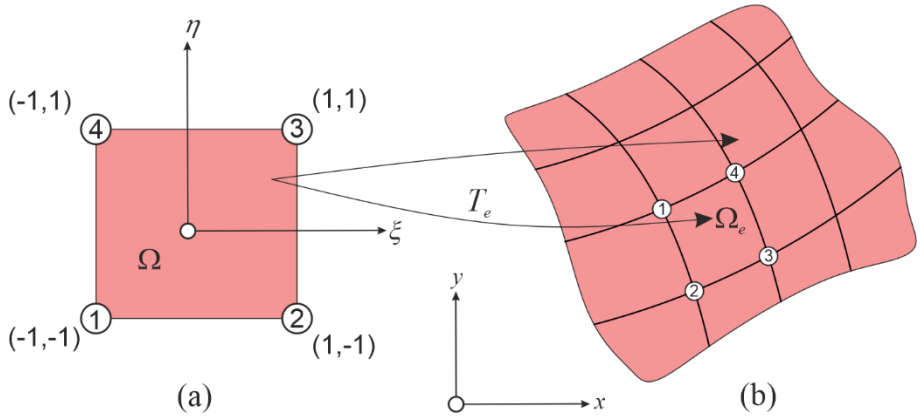

Figure 2 - Discretization of the shell domain (a) Master element in local coordinates (b) Shell domain in global coordinates

The resulting finite element system of equations of the laminated composite spherical shell can be represented in matrix form as follows:

$$\mathbf{KX} = \mathbf{F} \tag{13}$$

In Equation (13), $\mathbf{K}$ denotes the system matrix, $\mathbf{F}$ corresponds to the external force vector and $\mathbf{X}$ is the vector that contains the unknowns.

$$\mathbf{X}^i = \left[u^i \quad v^i \quad w^i \quad \theta_x^i \quad \theta_y^i \quad N_{xx}^i \quad N_{yy}^i \quad N_{xy}^i \quad M_{xx}^i \quad M_{yy}^i \quad M_{xy}^i \quad M_{xx}^{fi} \quad M_{yy}^{fi} \quad M_{xy}^{fi} \quad Q_{yz}^i \quad Q_{xz}^i\right]^T \tag{14}$$

When the system equation is solved, both displacement and stress resultant variables can be obtained directly at the nodes without any necessity for any post-processing step.

3. NUMERICAL RESULTS

The mixed finite element formulation proposed for laminated composite spherical and cylindrical shells is named MHST (Mixed Higher-Order Shell Theory), and a series of numerical examples are discussed to demonstrate its performance and effectiveness in stress resultants and displacement calculations under static loading, and the results are evaluated. The solutions are produced through a Fortran-based program developed by the authors. By

making comparisons with Khdeir et al. [51], who analytically solved Higher Order Shear Theory (HSDT), First Order Theory (FSDT) and Classical Theory (CST), Asadi et al. [14], who made FSDT and 3D finite element analysis solutions, analytical HSDT solutions of Sayyad and Ghugal [10] and Mantari et al. [11], CUF by Giunta et al. [13] and numerical FSDT solution of Hossain et al. [4] in the literature; the accuracy of the formulation and the developed program is tested. Various element meshes as $n_e = 8\times 8$, 16×16 , 20×20 and 26×26 were used in the examples. Afterwards, solutions for different loading and support conditions were presented. There are two types of materials (Material A and B) used in the examples. The engineering constants of those materials can be seen in Table 2:

Table 2 - Sample materials and mechanical properties

Engineering Constants	Materials	
	A	B
E_1	132379340029 [Pa]	25[GPa]
E_2	10755821377 [Pa]	1[GPa]
E_3	10755821377 [Pa]	1[GPa]
υ_{12}	0.24	0.25
υ_{13}	0.24	0.25
υ_{23}	0.49	0.25
G_{12}	5653700980.4 [Pa]	0.5[GPa]
G_{13}	5653700980.4 [Pa]	0.5[GPa]
G_{23}	3605958064.3 [Pa]	0.2[GPa]

3.1. [0/90/0] Cylindrical Shell with Various Boundary Conditions under Sinusoidal Load

A symmetrically laminated cylindrical shell is analyzed using the proposed mixed finite element formulation and its results are compared with the literature. The shell is under the influence of transverse load of function $p(x,y) = p_0 \sin(\pi x/a)\sin(\pi y/b)$ distributed over its outer surface (see Figure 1b). Here a and b are the arc-lengths of the shell in the x and y axes directions, respectively (see Figure 3). The curvature in the cylindrical shell is on the y axis, so $R_x = \infty$. The cross section is defined with the [0/90/0] material orientation, and each layer of equal thickness is considered to be formed with material A. The $\rho = a/h = 10$ value is considered as the shell length-thickness ratio.

In Table 3, the SSSS boundary condition (BC) indicates that all four edges of the shell are simply supported. According to SCSC boundary condition, the two edges of the shell in the x-axis direction are simply supported, while the other two edges in the y -axis direction are clamped. In order to evaluate the results presented in Table 3 in a general structure, the following non-dimensionalization process is carried out:

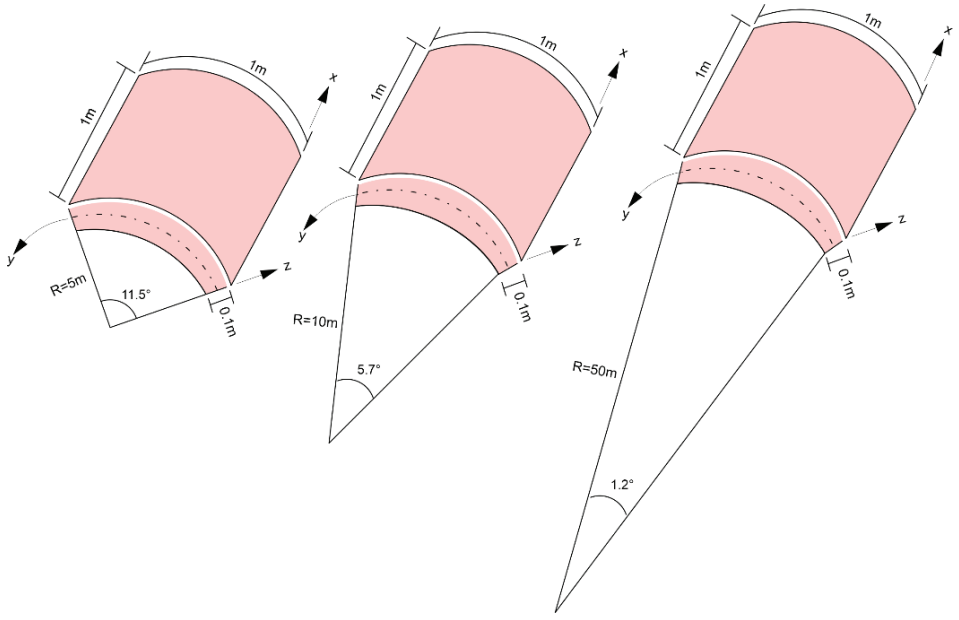

(a) *(b)* *(c)*

Figure 3 - The geometry of the cylindrical shells for (a) R/a=5 (b) R/b=10 (c) R/a=50

$$\overline{w} = \frac{10^2 E_2 h^3 w(a/2, b/2)}{p_0 a^4} \tag{15}$$

Table 3 - Convergence of laminated symmetrical cylindrical shell deflection under sinusoidal loading

BC'S	R/a	MHST (Touratier)				Khdeir et al. HSDT	HSDT – MHST percent Difference			
		8×8	16×16	20×20	26×26		8×8	16×16	20×20	26×26
SSSS	5	0.9354	0.9543	0.9561	0.9563	0.9524	1.78	-0.20	-0.39	-0.41
	10	0.9473	0.9668	0.9687	0.9689	0.9644	1.77	-0.25	-0.44	-0.47
	50	0.9512	0.9708	0.9728	0.9730	0.9683	1.77	-0.26	-0.46	-0.48
SCSC	5	0.4178	0.4200	0.4388	0.4407	0.4495	7.05	6.56	2.39	1.95
	10	0.4203	0.4346	0.4415	0.4435	0.4523	7.08	3.91	2.39	1.95
	50	0.4211	0.4395	0.4424	0.4444	0.4532	7.09	3.01	2.39	1.95

Table 4 - Deflection of the SSSS symmetrical cylindrical shell for several shear functions under sinusoidal loading

Formulation		Shear Function	R/a			MHST-HSDT percent Difference		
			5	10	50	5	10	50
MHST (Present)	20×20	Reissner	0.9546	0.9671	0.9711	-0.23	-0.27	-0.29
		Reddy	0.9546	0.9671	0.9711	-0.23	-0.27	-0.29
		Nguyen	0.9573	0.9699	0.9740	-0.51	-0.57	-0.58
Khdeir et al.		HSDT	0.9524	0.9644	0.9683			
		FSDT	0.9432	0.9550	0.9588			
		CST	0.7615	0.7694	0.7720			

Table 5 - Deflection of the SCSC symmetrical cylindrical shell applying several shear functions under sinusoidal loading

Formulation		Shear Function	R/a			MHST-HSDT percent Difference		
			5	10	50	5	10	50
MHST (Present)	26×26	Reissner	0.4400	0.4427	0.4436	2.12	2.12	2.12
		Reddy	0.4400	0.4427	0.4436	2.12	2.12	2.12
		Nguyen	0.4391	0.4418	0.4427	2.32	2.32	2.32
Khdeir et al.		HSDT	0.4495	0.4523	0.4424			
		FSDT	0.4357	0.4382	0.4391			
		CST	0.2047	0.2053	0.2055			

As can be seen in Table 3, the deflection values of the proposed numerical solution method (MHST) with the shear function of Touratier align very well with the Higher Order Theory (HSDT) results of the compared analytical method [51]. The results show consistent convergence behavior to an asymptotic value for both simply supported (SSSS) and mixed supported (SCSC) cases, however SSSS case demonstrates faster convergence behavior than SCSC (see Figures 4 and 5). The largest differences with the analytical results are seen in mixed supported case. That is why a finer mesh of 26×26 is applied. When the radius of the cylindrical shell increases, the percentage difference increases for the simply supported case, while it remains constant in the mixed supported case for the finer meshes (20×20 and 26×26). In Table 4, the deflection values of the SSSS symmetrical cylindrical shells (20×20) applying several shear functions under sinusoidal loading, are compared with Khdeir et al.'s analytical HSDT results. The percent differences of all the shear functions increase as the radius increases. The maximum MHST-HSDT percent difference (0.58) can be found in Nguyen Xuan et al.'s [48] shear function for the maximum radius. Therefore, 20×20 provides compatible results with the reference solution. In Table 5, the deflection values of the SCSC symmetrical cylindrical shells (26×26) applying several shear functions under sinusoidal loading, are compared with analytical results. Table 5 showed that both Reddy's [46] and Reissner's [47] shear functions produced uniform results (2.12 percent

difference from Khdeir et al. results), whereas the utilization of Nguyen Xuan et al.'s [48] shear function produced 2.32 percent difference for the same comparison parameter.

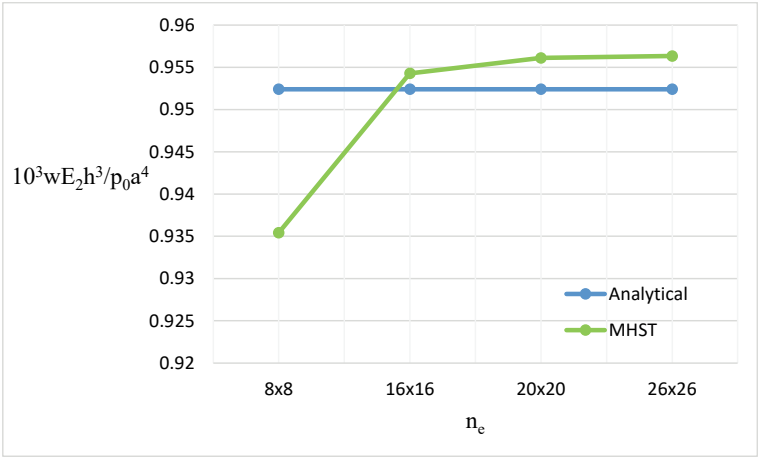

Figure 4 - The convergence behavior for the SSSS case

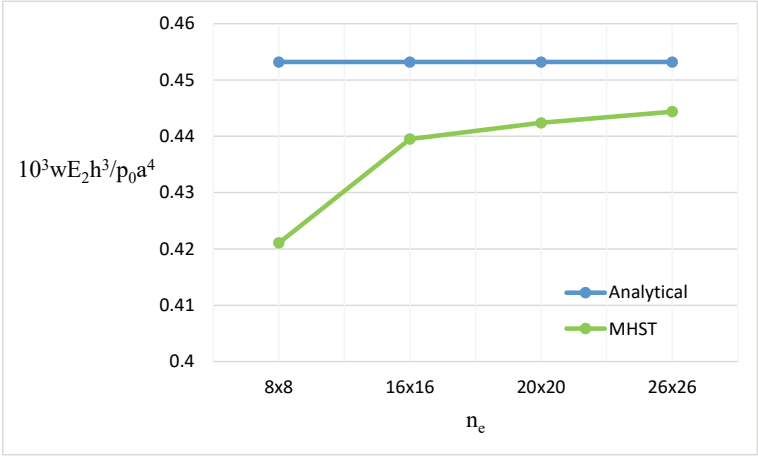

Figure 5 - The convergence behavior for the SCSC case

3.2. [0/90/0] Simply Supported Cylindrical Shell under Uniform Load

Uniformly $p(x)=p_0$ loaded simply supported cylindrical shells with [0/90/0] layouts are discussed in this section. In Table 6, MHST solutions in terms of the displacement, normal force, and moment values at the midpoint of the shell formed with material B are presented. The results obtained with the element meshes of 8×8, 16×16 and 20×20 for various thickness ratios ($\rho=a/h=10,20$) (see Figure 6) are compared with the FSDT and ANSYS

3D finite element solutions of Asadi et al. [14]. The non-dimensionalization of the values given in Table 6 is as follows:

$$\overline{w} = \frac{10^3 E_2 h^3 w(a/2, b/2)}{p_0 a^4}, \quad \overline{M} = \frac{10^3 M(a/2, b/2)}{p_0 a^2}, \quad \overline{N} = \frac{10^3 N(a/2, b/2)}{p_0 a^3} \tag{16}$$

Table 6 - Deflection and stress resultants in a uniformly loaded cylindrical shell

a/h	a/R	Theory	$\overline{w}$	$\overline{M_{xx}}$	$\overline{M_{yy}}$	$\overline{N_{xx}}$	$\overline{N_{yy}}$	3D-MHST Difference (percent)				
								$\overline{w}$	$\overline{M_{xx}}$	$\overline{M_{yy}}$	$\overline{N_{xx}}$	$\overline{N_{yy}}$
20	0.5	8×8	6.2771	104.04	7.41	587.56	576.78	1.57	2.15	4.05	1.43	0.01
		16×16	6.2533	102.76	7.35	583.04	573.50	1.94	0.89	4.72	2.18	0.58
		20×20	6.2477	102.55	7.35	582.54	572.92	2.03	0.68	4.72	2.27	0.68
		FSDT	6.1282	103.42	6.96	571.68	559.67					
		3D	6.3773	101.85	7.72	596.06	576.85					
	1	8×8	3.9190	64.18	3.36	737.56	723.53	0.29	3.08	13.8	0.08	0.62
		16×16	3.8617	62.77	3.33	723.96	713.41	1.74	0.83	12.7	1.92	0.79
		20×20	3.8551	62.600	3.33	722.75	712.23	1.91	0.55	12.8	2.08	0.95
		FSDT	3.8314	63.908	2.71	718.62	708.66					
		3D	3.9303	62.260	2.95	738.14	719.09					
10	0.5	8×8	10.147	114.89	12.5	237.62	223.68	4.82	2.08	10.0	4.87	0.52
		16×16	10.123	113.46	12.6	236.09	221.92	5.05	0.81	9.20	5.48	0.27
		20×20	10.116	113.26	12.5	235.94	221.69	5.11	0.63	9.27	5.54	0.37
		FSDT	9.5092	115.46	11.3	222.26	202.12					
		3D	10.661	112.55	13.9	249.78	222.52					
	1	8×8	8.2035	92.73	9.44	385.00	360.39	5.05	1.52	1.21	5.01	0.69
		16×16	8.1411	91.13	9.51	380.49	356.33	5.77	0.23	0.48	6.12	1.81
		20×20	8.1319	90.930	9.50	380.08	355.86	5.88	0.45	0.57	6.22	1.94
		FSDT	7.8418	95.117	7.94	367.19	335.23					
		3D	8.6399	91.340	9.56	405.29	362.88					

Table 6 shows that the results obtained from the current formulation (MHST) are highly compatible with the 3D solution. MHST results also exhibit a consistent convergence behavior depending on the increasing number of elements. It can be pointed out that when the shell becomes thinner, the differences (3D-MHST) in deflection values decrease. Among the stress resultants, the highest correlation is observed between $\overline{M_{xx}}$ values, whereas the

least correlation exists between $\overline{M_{yy}}$ values. This is an expected result because the shell curvature lies on the y -axis. Considering all comparison results, all predictions (except $\overline{M_{yy}}$ at $a/h=20$ and $a/R=1$) of MHST are in a better agreement with 3D solution compared to the predictions of the FSDT.

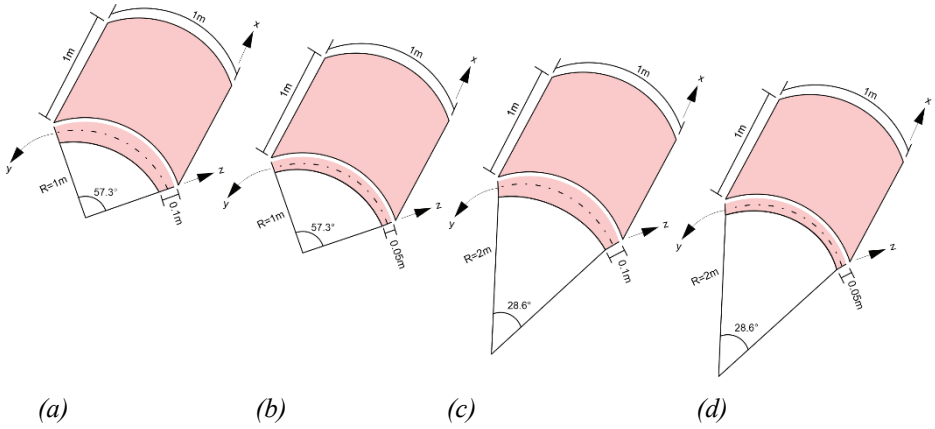

Figure 6 - The geometry of the cylindrical shells for (a) R/a=1 and a/h=10 (b) R/a=1 and a/h=20 (c) R/a=2 and a/h=10 (d) R/a=2 and a/h=20

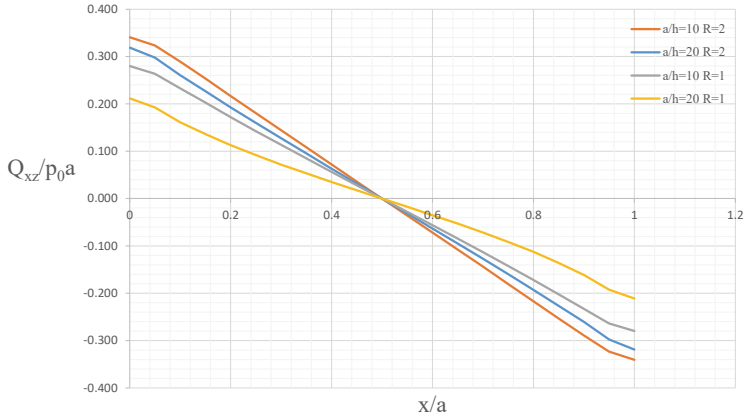

Figure 7 - Shear force distribution along the x -axis ($y=0.5$) in a simply supported symmetrical laminated cylindrical shell under uniform load (material B)

By exploiting the advantage of mixed finite element formulation, stress resultants are directly obtained at the nodes of the shell structures and presented in Figures 7-9. Figure 7 shows the shear force distribution in a uniformly loaded and simply supported laminated composite cylindrical shell discretized with 20×20 elements. The shear force becomes zero at the

symmetry axis as expected and takes varying values depending on the thickness ratio and radius of curvature. With increasing radius of curvature R_y, the shell behaves more like a plate so the absolute value of the shear force increases. Additionally, with increasing thickness, the shear force becomes more effective and has greater absolute values as can be easily followed in Figure 7.

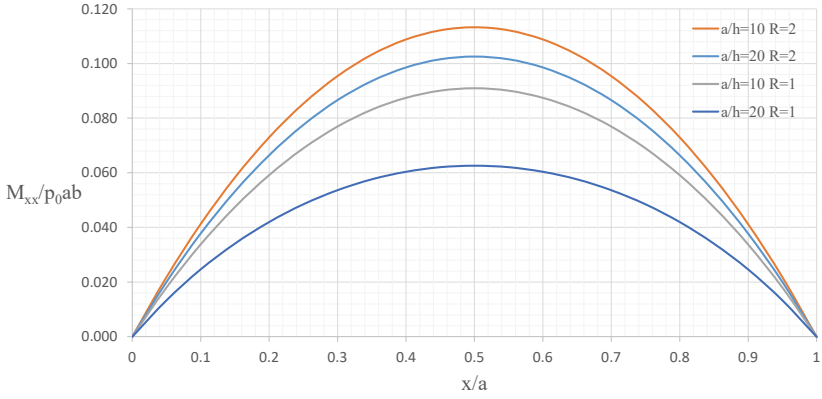

Figure 8 - Moment distribution along the x-axis ($y=0.5$) in a simply supported symmetrical laminated cylindrical shell under uniform load (material B)

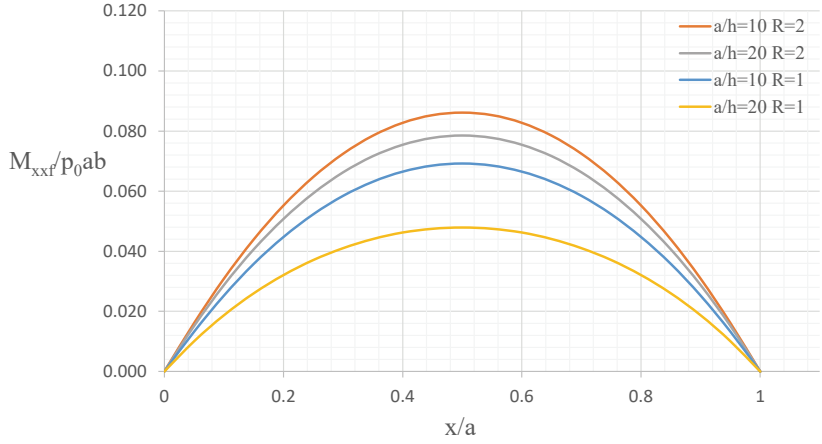

Figure 9 - Higher order moment distribution along the x-axis ($y=0.5$) in a simply supported symmetrical laminated cylindrical shell under uniform load (material B)

In the same shell problem, the moment distribution for different thickness ratios is given in Figure 8. In this distribution, dimensionless moment values for all thickness ratios demonstrate similar behavior to the shear force values given in Figure 7. The highest moment

value is obtained in the shell with the least curvature and the greatest thickness, while the lowest moment value is obtained in the thinnest shell structure with the highest curvature.

Higher-order moment distributions for the same shell with different thickness ratios are presented in Figure 9. High-order moment values along the shell's length are considerably lower than the normal moment values, but their distribution concerning thickness and radius is similar to that of the normal moment.

In Figures 10 and 11, dimensionless moment and shear force distributions for $\rho=10$ and $R=1$ are given for the entire domain. Since the curvature of the cylindrical shell is on the y -axis, the difference between $\overline{M_{xx}}$ and $\overline{M_{yy}}$ in Figure 10 and the difference between $\overline{Q_{xz}}$ and $\overline{Q_{yz}}$ in Figure 11 can be easily seen.

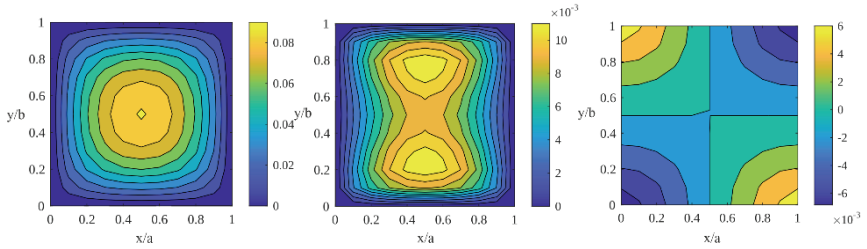

(a) (b) (c)

Figure 10 - Moment distribution on the $x-y$ axes for the symmetrical simply supported laminated cylindrical shell ($\rho=10$ and $R=1$) under uniform load, respectively (a) $\overline{M_{xx}}$ distribution (b) $\overline{M_{yy}}$ distribution (c) $\overline{M_{xy}}$ distribution

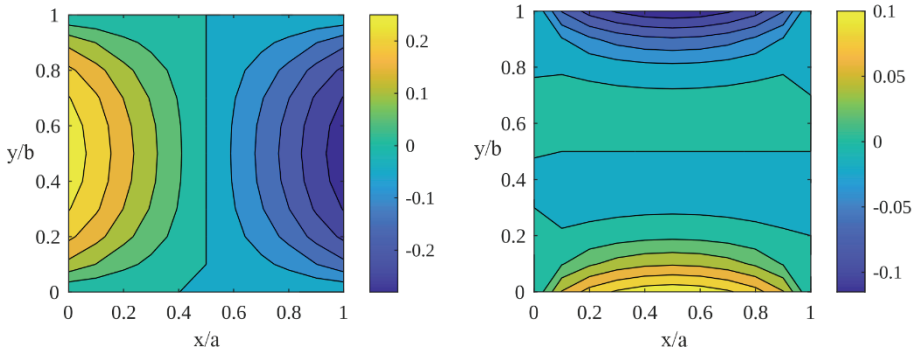

(a) (b)

Figure 11 - Shear force distribution on the $x-y$ axes for the symmetrical simply supported laminated cylindrical shell $(\rho=10$ and $R=1)$ under uniform load, respectively (a) $\overline{Q_{xz}}$ distribution (b) $\overline{Q_{yz}}$ distribution

3.3. [0/90/0] Simply Supported Spherical Shell under Sinusoidal Load

In this part, simply supported symmetrically laminated [0/90/0] spherical shells are statically investigated applying sinusoidal load ($p(x,y) = p_0 \sin(\pi x/a)\sin(\pi y/b)$). The spherical shell geometries are selected as $\rho = 10$ and $\rho = 100$ and the material is chosen as B (Table 2). R/a ratio is defined as 5, 10 and 100. The finest element mesh (20×20)is employed for the all deflection results. Reddy's and Touratier's shear functions are selected for the current analyses. The solutions are compared with PSDT (parabolic shear deformation theory which corresponds Reddy's shear function) and TSDT (trigonometric shear deformation theory which corresponds Touratier's shear function) conducted by Sayyad and Ghugal [10] , analytical HSDT of Mantari et al. [11], CUF of Giunta et al. [13] and numerical FSDT solution of Hossain et al. [4].

Table 7 - Deflection values for simply supported sinusoidally loaded spherical shell

a/h	R/a	MHST 20×20		Sayyad and Ghugal		Mantari et al.	Giunta et al.	Hossain et al.
		Reddy	Touratier	PSDT	TSDT			
10	5	0.6745	0.6794	0.6769	0.6819	0.6964	0.7312	0.6600
	10	0.7006	0.7060	0.7032	0.7086	0.7244	0.7497	0.6702
	100	0.7097	0.7152	0.7124	0.7179	0.7341	-	0.6699
100	5	0.1031	0.1031	0.1032	0.1032	0.1032	0.1036	0.1035
	10	0.2405	0.2405	0.2410	0.2410	0.2413	0.2416	0.2415
	100	0.4291	0.4292	0.4307	0.4307	0.4318	-	0.4303

It can be concluded from Table 7 that current formulation's deflection values are match well all referenced solutions. The most consistent results can be mentioned as MHST(Reddy)-PSDT and MHST(Touratier)-TSDT. This is a predictable solution due to the utilization of the same shear functions.

3.4. [0/90/0] Simply Supported Spherical Shell under Uniform Load

In this section, the problem specified in Section 3.3 is solved under uniform loading condition. The spherical shell thickness ratio is selected as $\rho = 10$. $R/a = 20$ and $R/a = 50$ ratios are considered to examine different geometric configurations. In Table 8, the results are compared with Sayyad and Ghugal and the percent differences are specified for MHST(Reddy)-PSDT and MHST(Touratier)-TSDT. The percentage differences in both comparisons are almost identical. A slight difference is observed when the R/a ratio is increased from 20 to 100.

Table 8 - Deflection values for simply supported uniformly loaded spherical shell

a/h	R/a	MHST 20 x 20		Sayyad and Ghugal		Percent Differences	
		Reddy	Touratier	PSDT	TSDT	Reddy-PSDT	Touratier-TSDT
10	5	1.0344	1.0422	1.0333	1.0411	0.11	0.11
	10	1.0763	1.0848	1.0752	1.0837	0.10	0.10
	20	1.0872	1.0959	1.0862	1.0949	0.10	0.09
	50	1.0904	1.0991	1.0894	1.0980	0.09	0.10
	100	1.0908	1.0995	1.0898	1.0985	0.09	0.89

4. CONCLUSION

In this study, the displacement and stress resultant distributions of laminated composite spherical and cylindrical shells under different boundary and loading conditions are examined. For this purpose, a mixed finite element method is adopted based on the Higher Order Shear Theory. Four different shear functions are considered for the Higher Order Theory. Finite element equations obtained using the Hellinger-Reissner variational principle are discretized using two-dimensional four-node elements with C_0 continuity. As an advantage of the mixed finite element method, force and moment components, as well as displacement type field variables can be calculated directly at the nodes. Convergence and comparison analyses are performed on the problems discussed and it was observed that the results are in good agreement with the reference analytical, numerical and 3D solutions. In addition, taking into account different thickness and depth characteristics of the cylindrical composite shell; shear force, moment and higher order moment values are compared. It has been observed that the results obtained for the current formulation are highly compatible with many advanced finite element solutions featured in the literature and sometimes produce better results, especially in moment calculations. It is thought that the proposed formulation offers the opportunity to be developed for many types of analysis in the future and adapted to various problems.

Symbols

$\delta \Pi_{HR}$: First variation of the functional

a : Shell length

b : Shell width

$\boldsymbol{\varepsilon}^{\mathbf{u}}$: Strain vector in terms of displacement components

$\boldsymbol{\varepsilon}^{\boldsymbol{\sigma}}$: Strain vector in terms of the stress components

$\boldsymbol{\sigma}^{\boldsymbol{\sigma}}$: Stress vector

δ : Variational operator

$\hat{\mathbf{t}}$: Traction vector

Γ : Boundary of the structure

E_1, E_2, E_3 : Young's moduli

v_{ij} : Poison's ratio

G_α : Shear moduli ($\alpha = 23,31,12$)

$f(z)$: Shear functions

h : Thickness

z : Any coordinate along the thickness

$\theta_x(x)$: Shear rotation about y axis

$\theta_y(x)$: Shear rotation about y axis

σ_{ii} : In-plane stress components

σ_{ij} : Transverse shear stress components

N_{ii} : In-plane force resultant of stress components

M_{ii} : Resultant moment of stress components

M_{ii}^f : Resultant higher order moment of stress components

Q_{ij} : Resultants of transverse shear stress components

$\mathbf{e^u}$: Strain measures in terms of kinematical variables

$\mathbf{E}$: Section stiffness matrix

$\mathbf{e^P}$: Strain measures in terms of stress resultants

$\mathbf{F}$: External force vector

$\mathbf{K}$: System matrix

$\mathbf{p}$: Applied load vector

$\mathbf{P}$: Stress resultants

$\mathbf{X}$: Unknown vector

References

[1] M. Dorduncu, Peridynamic modeling of delaminations in laminated composite beams using refined zigzag theory, Theoretical and Applied Fracture Mechanics 112 (2021) 102832. https://doi.org/10.1016/j.tafmec.2020.102832.

[2] M. Dorduncu, Stress analysis of laminated composite beams using refined zigzag theory and peridynamic differential operator, Composite Structures 218 (2019) 193–203. https://doi.org/10.1016/j.compstruct.2019.03.035.

[3] J.N. Reddy, K. Chandrashekhara, Geometrically non-linear transient analysis of laminated, doubly curved shells, International Journal of Non-Linear Mechanics 20 (1985) 79–90. https://doi.org/10.1016/0020-7462(85)90002-2.

[4] S.J. Hossain, P.K. Sinha, A.H. Sheikh, A finite element formulation for the analysis of laminated composite shells, Computers & Structures 82 (2004) 1623–1638. https://doi.org/10.1016/j.compstruc.2004.05.004.

[5] E. Asadi, M.S. Qatu, Static analysis of thick laminated shells with different boundary conditions using GDQ, Thin-Walled Structures 51 (2012) 76–81. https://doi.org/10.1016/j.tws.2011.11.004.

[6] A.A. Khdeir, Comparative dynamic and static studies for cross-ply shells based on a deep thick shell theory, IJVNV 7 (2011) 306. https://doi.org/10.1504/IJVNV.2011.043192.

[7] S.M. Mousavi, M. Aghdam, Static bending analysis of laminated cylindrical panels with various boundary conditions using the differential cubature method, J. Mech. Mater. Struct. 4 (2009) 509–521. https://doi.org/10.2140/jomms.2009.4.509.

[8] B. Sobhaniaragh, R.C. Batra, W.J. Mansur, F.C. Peters, Thermal response of ceramic matrix nanocomposite cylindrical shells using Eshelby-Mori-Tanaka homogenization scheme, Composites Part B: Engineering 118 (2017) 41–53. https://doi.org/10.1016/j.compositesb.2017.02.032.

[9] J.N. Reddy, C.F. Liu, A higher-order shear deformation theory of laminated elastic shells, International Journal of Engineering Science 23 (1985) 319–330. https://doi.org/10.1016/0020-7225(85)90051-5.

[10] A.S. Sayyad, Y.M. Ghugal, Static and free vibration analysis of laminated composite and sandwich spherical shells using a generalized higher-order shell theory, Composite Structures 219 (2019) 129–146. https://doi.org/10.1016/j.compstruct.2019.03.054.

[11] J.L. Mantari, A.S. Oktem, C. Guedes Soares, Static and dynamic analysis of laminated composite and sandwich plates and shells by using a new higher-order shear deformation theory, Composite Structures 94 (2011) 37–49. https://doi.org/10.1016/j.compstruct.2011.07.020.

[12] A. Kumar, A. Chakrabarti, M. Ketkar, Analysis of laminated composite skew shells using higher order shear deformation theory, Lat. Am. j. Solids Struct. 10 (2013) 391–919. https://doi.org/10.1590/S1679-78252013000500003.

[13] G. Giunta, F. Biscani, S. Belouettar, E. Carrera, Hierarchical modelling of doubly curved laminated composite shells under distributed and localised loadings, Composites Part B 42 (2011) 682–91. https://doi.org/10.1016/j.compositesb.2011.02.002.

[14] E. Asadi, W. Wang, M.S. Qatu, Static and vibration analyses of thick deep laminated cylindrical shells using 3D and various shear deformation theories, Composite Structures 94 (2012) 494–500. https://doi.org/10.1016/j.compstruct.2011.08.011.

[15] H.L. Ton-That, H. Nguyen-Van, T. Chau-Dinh, An Improved Four-Node Element for Analysis of Composite Plate/Shell Structures Based on Twice Interpolation Strategy, Int. J. Comput. Methods 17 (2020) 1950020. https://doi.org/10.1142/S0219876219500208.

[16] H. Zuo, Y. Chen, F. Jia, Z. Yang, Unified wavelet finite element formulation for static and vibration analysis of laminated composite shells, Composite Structures 272 (2021) 114207. https://doi.org/10.1016/j.compstruct.2021.114207.

[17] M. Yaghoubshahi, E. Asadi, S.J. Fariborz, A higher-order shell model applied to shells with mixed boundary conditions, Proceedings of the Institution of Mechanical Engineers, Part C: Journal of Mechanical Engineering Science 225 (2011) 292–303. https://doi.org/10.1243/09544062JMES2050.

[18] R.M.J. Groh, P.M. Weaver, Static inconsistencies in certain axiomatic higher-order shear deformation theories for beams, plates and shells, Composite Structures 120 (2015) 231–245. https://doi.org/10.1016/j.compstruct.2014.10.006.

[19] K. Bhaskar, T.K. Varadan, A higher-order theory for bending analysis of laminated shells of revolution, Computers & Structures 40 (1991) 815–819. https://doi.org/10.1016/0045-7949(91)90310-I.

[20] T.N. Doan, D. Van Thom, N.T. Thanh, P. Van Chuong, N.C. Tho, N.T. Ta, H.N. Nguyen, Analysis of stress concentration phenomenon of cylinder laminated shells using higher-order shear deformation Quasi-3D theory, Composite Structures 232 (2020) 111526. https://doi.org/10.1016/j.compstruct.2019.111526.

[21] E. Viola, F. Tornabene, N. Fantuzzi, Static analysis of completely doubly-curved laminated shells and panels using general higher-order shear deformation theories, Composite Structures 101 (2013) 59–93. https://doi.org/10.1016/j.compstruct.2013.01.002.

[22] I.F. Pinto Correia, C.M. Mota Soares, C.A. Mota Soares, J. Herskovits, Analysis of laminated conical shell structures using higher order models, 62 (2003) 383–390. https://doi.org/10.1016/j.compstruct.2003.09.009.

[23] F. Tornabene, N. Fantuzzi, E. Viola, R.C. Batra, Stress and strain recovery for functionally graded free-form and doubly-curved sandwich shells using higher-order equivalent single layer theory, Composite Structures 119 (2015) 67–89. https://doi.org/10.1016/j.compstruct.2014.08.005.

[24] M. Yaqoob Yasin, S. Kapuria, An efficient layerwise finite element for shallow composite and sandwich shells, Composite Structures 98 (2013) 202–214. https://doi.org/10.1016/j.compstruct.2012.10.048.

[25] A. Gupta, S. Pradyumna, Geometrically nonlinear bending analysis of variable stiffness composite laminated shell panels with a higher-order theory, Composite Structures 276 (2021) 114527. https://doi.org/10.1016/j.compstruct.2021.114527.

[26] G.M. Kulikov, S.V. Plotnikova, Advanced formulation for laminated composite shells: 3D stress analysis and rigid-body motions, Composite Structures 95 (2013) 236–246. https://doi.org/10.1016/j.compstruct.2012.07.020.

[27] M.S. Qatu, A. Algothani, Bending analysis of laminated plates and shells by different methods, Computers & Structures 52 (1994) 529–539. https://doi.org/10.1016/0045-7949(94)90238-0.

[28] E.E. Karataş, R.F. Yükseler, Snap-through Buckling of Shallow Spherical Shells under Ring Loads, Teknik Dergi 32 (2021) 10695–10716. https://doi.org/10.18400/tekderg.565095.

[29] A. Sofiyev, A. Deniz, M. Avcar, P. Özyigit, M. Omurtag, Effects of the non-homogeneity and elastic medium on the critical torsional load of the orthotropic cylindrical shell footnotemark, Acta Physica Polonica A 123 (2013) 728–730.

[30] A. Yadav, M. Amabili, S. Kumar Panda, T. Dey, Instability analysis of fluid-filled angle-ply laminated circular cylindrical shells subjected to harmonic axial loading | Elsevier Enhanced Reader, European Journal of Mechanics - A/Solids 97 (2023). https://doi.org/10.1016/j.euromechsol.2022.104810.

[31] M.C. Ray, Exact solutions of elasticity theories for static analysis of doubly curved antisymmetric angle-ply composite shells, Mechanics of Advanced Materials and Structures (2023) 1–15. https://doi.org/10.1080/15376494.2023.2246223.

[32] Md.I. Alam, M.K. Pandit, A.K. Pradhan, A modified higher-order zigzag theory for predicting flexural behavior of laminated composite and sandwich shell, Mechanics of Advanced Materials and Structures (2023) 1–16. https://doi.org/10.1080/15376494.2023.2231445.

[33] A.B. Arumugam, M. Subramani, M. Dalakoti, P. Jindal, R. Selvaraj, E. Khalife, Dynamic characteristics of laminated composite CNT reinforced MRE cylindrical sandwich shells using HSDT, Mechanics Based Design of Structures and Machines 51 (2023) 4120–4136. https://doi.org/10.1080/15397734.2021.1950550.

[34] A. Ozutok, E. Madenci, Static analysis of laminated composite beams based on higher-order shear deformation theory by using mixed-type finite element method, Int. J. Mech. Sci. 130 (2017) 234–243. https://doi.org/10.1016/j.ijmecsci.2017.06.013.

[35] A. Kutlu, M. Dorduncu, T. Rabczuk, A novel mixed finite element formulation based on the refined zigzag theory for the stress analysis of laminated composite plates, Composite Structures 267 (2021) 113886. https://doi.org/10.1016/j.compstruct.2021.113886.

[36] A. Kutlu, Mixed finite element formulation for bending of laminated beams using the refined zigzag theory, Proceedings of the Institution of Mechanical Engineers, Part L: Journal of Materials: Design and Applications 235 (2021) 1712–1722. https://doi.org/10.1177/14644207211018839.

[37] A. Kutlu, G. Meschke, M.H. Omurtag, A new mixed finite-element approach for the elastoplastic analysis of Mindlin plates, J Eng Math 99 (2016) 137–155. https://doi.org/10.1007/s10665-015-9825-7.

[38] U.N. Aribas, M. Ermis, N. Eratli, M.H. Omurtag, The static and dynamic analyses of warping included composite exact conical helix by mixed FEM | Elsevier Enhanced Reader, Composites Part B: Engineering 160 (2019) 285–297. https://doi.org/10.1016/j.compositesb.2018.10.018.

[39] U.N. Aribas, M. Ermis, A. Kutlu, N. Eratli, M.H. Omurtag, Forced vibration analysis of composite-geometrically exact elliptical cone helices via mixed FEM, Mechanics of Advanced Materials and Structures (2020) 1–19. https://doi.org/10.1080/15376494.2020.1824048.

[40] U.N. Aribas, M. Ermis, M.H. Omurtag, The static and stress analyses of axially functionally graded exact super-elliptical beams via mixed FEM, Arch Appl Mech 91 (2021) 4783–4796. https://doi.org/10.1007/s00419-021-02033-w.

[41] A. Kutlu, M. Hakkı Omurtag, Large deflection bending analysis of elliptic plates on orthotropic elastic foundation with mixed finite element method, International Journal of Mechanical Sciences 65 (2012) 64–74. https://doi.org/10.1016/j.ijmecsci.2012.09.004.

[42] M.H. Omurtag, A.Y. Aköz, Isoparametric mixed finite element formulation of orthotropic cylindrical shells, Computers & Structures 55 (1995) 915–924. https://doi.org/10.1016/0045-7949(94)00450-H.

[43] Y. Bab, A. Kutlu, Mixed finite element formulation based on higher order theory for stress calculation of laminated composite beams, in: Proceedings 22. National Mechanics Congress, Adana, Turkey, 2021.

[44] Y. Bab, A. Kutlu, Stress analysis of laminated HSDT beams considering bending extension coupling, Turkish Journal of Civil Engineering 34 (2023) 1–23. https://doi.org/10.18400/tjce.1206777.

[45] M. Touratier, An efficient standard plate theory, International Journal of Engineering Science 29 (1991) 901–916. https://doi.org/10.1016/0020-7225(91)90165-Y.

[46] J.N. Reddy, A simple higher-order theory for laminated composite plates, Journal of Applied Mechanics 51 (1984) 745–752. https://doi.org/10.1115/1.3167719.

[47] E. Reissner, On transverse bending of plates, including the effect of transverse shear deformation, International Journal of Solids and Structures 11 (1974) 569–573.

[48] H. Nguyen-Xuan, C.H. Thai, T. Nguyen-Thoi, Isogeometric finite element analysis of composite sandwich plates using a higher order shear deformation theory, Composites Part B: Engineering 55 (2013) 558–574. https://doi.org/10.1016/j.compositesb.2013.06.044.

[49] J.N. Reddy, Mechanics of Laminated Composite Plates and Shells, CRC Press, Boca Raton, 2003.

[50] Y. Bab, Mixed finite element formulations for laminated beams and plates based on higher order shear deformation theories, Master's Thesis, Istanbul Technical University, 2021.

[51] A.A. Khdeir, L. Librescu, D. Frederick, A shear deformable theory of laminated composite shallow shell-type panels and their response analysis II: Static response, Acta Mechanica 77 (1989) 1–12. https://doi.org/10.1007/BF01379740.